Mechanisms for NH_3 Decomposition on Si(100) – (2 × 1) Surface: A Quantum Chemical Cluster Model Study

Xin Xu,*[a] Song-Yun Kang,[b] and Tokio Yamabe[c]

Abstract: In this paper, we present a detailed mechanism for the complete decomposition of NH_3 to NH_x(a) ($x = 0-2$). Our calculations show that the initial decomposition of NH_3 to NH_2(a) and H(a) is facile, with a transition-state energy 7.4 kcal mol^{-1} below the vacuum level. Further decomposition to N(a) or recombination – desorption to NH_3(g) is hindered by a large barrier of $\sim$46 kcal mol^{-1}. There are two plausible NH_2 decomposition pathways: 1) NH_2(a) insertion into the surface Si–Si dimer bond, and 2) NH_2(a) insertion into the Si–Si backbond. We find that pathway (1) leads to the formation of a surface Si=N unit, similar to a terminal Si=N_t pair in silicon nitride, Si_3N_4, while pathway (2) leads to the formation of a near-planar, subsurface Si_3N unit, in analogy to a central nitrogen atom (N_c) bounded to three silicon atoms in the Si_3N_4 environment. Based on these results, a plausible microscopic mechanism for the nitridation of the Si(100) – (2 × 1) surface by NH_3 is proposed.

Keywords: chemisorption · density functional calculations · reaction mechanisms · silicon · surface chemistry

Introduction

The reaction of ammonia with silicon surfaces has been the subject of intensive investigations, due to its technological importance. The industrial production processes involve reactions between NH_3 and SiH_4 with Si surfaces in the temperature range from 700 – 900 °C or exposing the Si surface to NH_3 at 1000 – 1100 °C.[1] These reactions serve as a method for growing thin films of silicon nitride on crystalline silicon wafers, which can be used as a passivating and an insulating barrier for a variety of devices, such as mechanical and optical transducers,[2] and integrated solid-state sensors.[3]

Various experimental techniques have been applied to delineate the reaction mechanisms.[4] Based on their results from ion-scattering spectroscopy and X-ray photoelectron spectroscopy (XPS),[4, 5] Avouris et al. reported that ammonia undergoes a complete dissociation on the (100) surface, even at 90 K, and that the chemisorbed H's saturate the surface dangling bonds while nitrogens occupy the subsurface sites. These conclusions were confirmed by other studies from the same group, using ultraviolet photoelectron spectroscopy (UPS) and scanning – tunneling microscopy (STM),[5, 6] although their later XPS and UPS studies concluded that NH_3 dissociates at 300 K to form the NH(a) and H(a) species on the Si(100) – (2 × 1) surface.[7]

Contrary to these conclusions, however, more recent XPS,[8] UPS,[9] electron energy-loss spectra (EELS),[10] high-resolution EELS (HREELS),[11, 12] electron-stimulated-desorption ion angular distribution (ESDIAD),[13] static secondary ion mass spectroscopy (SSIMS),[14] and scanned-energy mode X-ray photoelectron diffraction study (XPD)[15] have proposed that NH_2(a) and H(a) are the only species produced upon ammonia adsorption at room temperature. The Si–N bond length of the $SiNH_2$ group was found to be 1.73 ± 0.08 Å, with a bond angle relative to the surface normal of 21 ± 4°.[15]

It was found that the NH_2(a) thus produced is stable up to more than 600 K.[8–15] Above 600 K, NH_2(a) either recombines with H(a) to produce NH_3(g), or dissociates to N(a), followed by H_2(g) liberation and surface N(a) penetration into the bulk at around 750 K.[8–15] On one hand, Chen et al., based on the H_2 desorption yield, reported that $\sim$73 % of NH_2(a) desorbs as NH_3(g) through surface recombination, while $\sim$27 % undergoes full dissociation on the surface.[12] On the other hand, Dresser concluded that dissociation is the main channel, and recombination – desorption is a minor channel since the

[a] Prof. X. Xu
State key Laboratory for Physical Chemistry of Solid Surfaces
Department of Chemistry, Institute of Physical Chemistry
Xiamen University, Xiamen 361005 (China)
Fax: (+86) 592-2183047
E-mail: xinxu@xmu.edu.cn

[b] Dr. S.-Y. Kang
Department of Molecular Engineering, Kyoto University
Kyoto 606-8501 (Japan)

[c] Prof. T. Yamabe
Nagasaki Institute of Applied Science
536 Aba-machi, Nagasaki, 851-0193 (Japan)

Supporting information for this article is available on the WWW under http://www.chemeurj.org or from the author.

  0947-6539/02/0823-5351 $ 20.00+.50/0

N/Si AES (Auger Electron Spectroscopy) ratio shows negligible change.[13]

The TPD (temperature-programmed desorption) experiment gave the activation energy of the associated desorption of NH_3 as 46 kcal mol^{-1}.[13] By assuming the decrease of the $SiNH_2^+$ SSIMS signal between 630 and 730 K to be only decomposition of NH_2(a), Zhou et al. obtained an activation energy of 30 ± 4 kcal mol^{-1} for NH_2(a) decomposition on Si(100).[14] Kubler et al. measured the surface-nitrogen concentration Q_N based on their XPS studies. An Arrhenius plot of the nitrogen uptake Q_N led to an apparent activation energy of 4.3 kcal mol^{-1};[8, 9] this indicated an activation energy of 50.4 kcal mol^{-1} for the NH_2(a) decomposition.

The way that nitride grows on the surface during thermal nitridation is not fully understood. The proposed mechanisms involve layer-by-layer growth,[16] island growth,[17] and lateral growth.[18] Despite the wealth of attention paid to this system, an unambiguous mechanistic understanding is lacking.

Besides two early calculations,[19, 20] there have been many new calculations at the state-of-the-art level on the NH_3/Si(100)$-(2\times1)$ system,[21–27] by using the CASSCF/MRSDCI (complete active-space self-consistent field/multireference single- and double-excitation configuration interaction) cluster model,[21] gradient-corrected density functional theory (DFT) with the Becke three-parameter exchange[28] functional and the Lee–Yang–Parr correlation functional[29] (B3LYP) cluster model,[24–27] and slab model calculations with DFT of the local-density approximation (LDA)[22] or the generalized gradient approximation (GGA).[23] Only NH_3(a) molecular adsorption and the initial decomposition to NH_2(a) and H(a) have been addressed by these calculations.[20–27] The molecular adsorption energy was predicted to be 33 kcal mol^{-1}[21] by MRSDCI and 27.0 kcal mol^{-1}[27] by B3LYP with cluster model, and 28 kcal mol^{-1}[23] by GGA/Slab mode. The activation energy for N–H bond cleavage of NH_3(a) to form NH_2(a) and H(a) was found to be around 15,[21] 19,[27] and 16[23] kcal mol^{-1}, respectively, by these three methods. The whole reaction exothermicity from NH_3(g) to NH_2(a) and H(a) is -75 kcal mol^{-1} by MRSDCI,[21] -58 kcal mol^{-1} by B3LYP,[27] and -46 kcal mol^{-1} by GGA.[23] All theories predicted that $NH_3(a) \rightarrow NH_2(a) + H(a)$ proceeds below the vacuum level. Hence the decomposition of NH_3 on Si(100)$-(2\times1)$ to NH_2(a) and H(a) is not an activated process. Further decomposition of NH_2(a) was not studied by these calculations.[20–27]

In this paper, we present a detailed mechanism for the complete decomposition of NH_3 to NH_x(a) ($x = 0-2$). Three kinds of elementary processes, namely N–H bond cleavage, NH_x insertion, and H_2 liberation, are investigated. Based on these results, a plausible microscopic mechanism for the nitridation of the Si(100)$-(2\times1)$ surface by NH_3 is proposed.

Computational Methods

Our approach is based on unrestricted B3LYP.[28, 29] It consists of the Slater local exchange, the nonlocal exchange of Becke 88, the exact exchange, the local correlation functional of Vosco–Wilk–Nusair, and the nonlocal correlation functional of Lee–Yang–Parr. The contribution of each energy to the B3LYP energy expression was fitted empirically on a reference set of molecules. Such a method has been demonstrated to have an accuracy of ~ 3 kcal mol^{-1} for simple molecules.[30] In particular, Nachtigall et al. found that the B3LYP functional gave a close agreement with their quadratic CI calculations in the study of hydrogen desorption from the monohydride phase of the Si(100)$-(2\times1)$ surface.[31] Nevertheless, a lot of bond breaking and forming is involved in the transition states. Larger errors in predicting the reaction barriers should be anticipated than those in calculating the thermochemistry with B3LYP.

A Si_9H_{12}-cluster model was used in the present study. It consists of two surface-layer Si atoms (Si1) representing a surface dimer, four second-layer Si atoms (Si2), two third-layer Si atoms (Si3), and one fourth-layer Si atom (Si4). In spite of its simplicity, in that it neglects the nonlocal effect during adsorption, this single-dimer model gives reasonable energetic and geometric predictions.[21, 24–27] However, reaction mechanisms involving neighboring dimers cannot be explored.

The complete geometry optimization (with no constrained degree of freedom) was done by using analytical gradients. In the free Si_9H_{12} cluster, the dimer bond length Si1–Si1 is optimized to be 2.242 Å, which is shorter than the Si1–Si2 (2.350 Å) bond length between the first- and second-layer substrate atoms. These numbers compare well with the experiment data of 2.24 ± 0.08 Å for the dimer bond[39] and 2.352 Å for the Si–Si separation in the bulk.[40] In fact, we find that the optimized Si3–Si4 bond length in every cluster model studied here is within 2.36–2.38 Å, which compares well with the experimental bulk Si–Si lengths. This indicates that the nitridation process is quite a localized surface phenomenon, and justifies our use of a cluster model. For a detailed investigation on the cluster-size effect and the effect of a constrained optimization versus a full optimization for the NH_3/Si(100)$-(2\times1)$ system, we refer to Ref. [26].

Vibrational frequencies were calculated analytically to ensure that each minimum was a true local minimum (only real frequencies) and that each transition state has only a single imaginary frequency (negative eigen-value of the Hessian). The basis set used on all atoms for geometry optimizations and vibrational-frequency calculations was the standard 6–31G**.[32, 33] Unscaled zero-point-energies (ZPE) were evaluated at the B3LYP/6–31G** level. Single-point energy calculations were carried out at the 6–31G** optimized geometries with the cc-pVTZ basis sets.[34–36]

All calculations were carried out with the Gaussian 98 suite of programs.[37]

Results

1. Formation of surface N(a): HSi1-N=Si1(P1): Figure 1 shows the reaction pathway for the formation of the surface HSi1-N=Si1 (P1). The important geometrical parameters can be found in Table S1 of the Supporting Information. The adsorption and reaction from R1 (the free adsorbate NH_3(g) + the bare Si_9H_{12} cluster, denoted as NH_3(g) + Si1=Si1), through a molecularly adsorbed precursor state, LM1 ($NH_3\cdots$Si1–Si1: where "$\cdots$" denotes a dative bond and ":" denotes a lone pair of electrons), to the initial decomposition products NH_2(a) and H(a), LM2 (NH_2-Si1-Si1-H), have been well studied.[21–27] Consistent with previous studies, LM1 is found to be bound by 21.6 kcal mol^{-1} with respect to the vacuum level, R1. There is a barrier, 14.2 kcal mol^{-1}, separating the molecular adsorption state LM1 from the dissociative state LM2. The whole process from R1 to LM2 proceeds below the vacuum level. Hence the initial decomposition of NH_3 on Si(100)$-(2\times1)$ to NH_2(a) + H(a) is not activated.[21] The whole energetics from R1 to LM2 is found to be -53.1 kcal mol^{-1}, which can be compared with the experimental value of -46 kcal mol^{-1} for the activation energy of associative desorption of NH_2(a).[13] We calculated that TS1 is

0947-6539/02/0823-5352 $ 20.00+.50/0 *Chem. Eur. J.* **2002**, *8*, No. 23

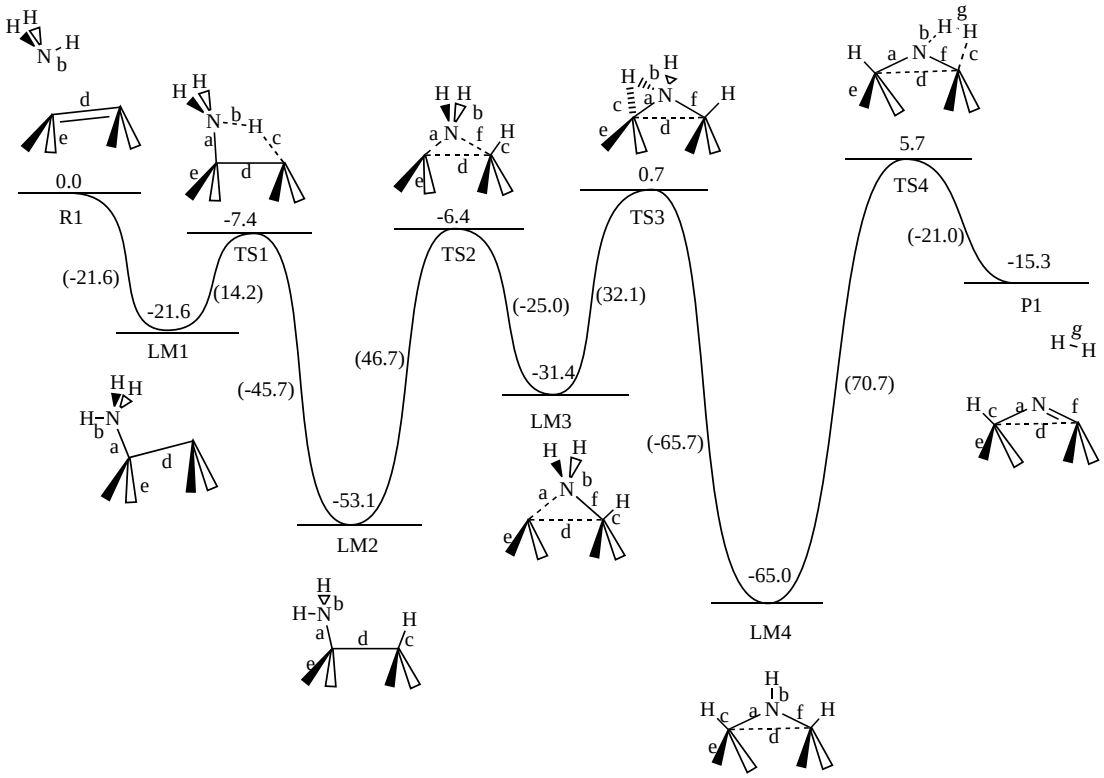

Figure 1. Mechanism for the formation of surface product P1 (HSi1-N=Si1). The key step is NH_2 insertion into the surface Si1–Si1 dimer bond, followed by H_2 liberation from LM4 (H-Si1-NH-Si1-H).

Table 1. N–H bond-decomposition barrier [kcal mol^{-1}].

Reactions	Figure		E_a
LM1 → LM2	1	(NH_3 ··· Si1–Si1:) → (NH_2-Si1-Si1-H)	14.2
LM11 → P2	3	(($Si2)_2$-NH ··· :Si1H–Si1H) → (($Si2)_2$-N-Si1H_2-Si1H)	26.2
LM23 → LM24	6	(($Si2)_2$-NH ··· :Si1H–Si1•) → (($Si2)_2$-N-Si1H_2-Si1•)	27.2
LM9 → LM10	3	(Si2-NH_2 ··· :Si1–Si1H) → (Si2-NH-Si1H-Si1H)	31.0
LM21 → LM22	6	(Si2-NH_2 ··· :Si1–Si1•) → (Si2-NH-Si1H-Si1•)	31.2
LM3 → LM4	1	(:Si1 ··· NH_2–Si1H) → (H-Si1-NH-Si1-H)	32.1
LM18 → LM19	5	(:Si1 ··· NH_2–Si1•) → (H-Si1-NH-Si1•)	33.4
LM17 → LM25		(NH_2-Si1-Si1•) → (•NH-Si1-Si1-H)	48.1
LM28 → LM29	8	(Si2-NH-Si1-Si1H) → (Si2-N-Si1H-Si1H)	48.1
LM5 → P1	2	(•Si1-NH-Si1•) → (H-Si1-N=Si1)	54.1
LM2 → LM7	2	(NH_2-Si1-Si1-H) → (H-N=Si1, H-Si1-H)	57.6

7.4 kcal mol^{-1} below R1. The corresponding experimental value was estimated to be around 4 kcal mol^{-1}.[38]

The molecular precursor LM1 (NH_3 ··· Si1–Si1:) is characterized by a long Si1 ··· NH_3 dative bond of 2.014 Å. The Si1–NH_2 bond in LM2 (NH_2-Si1-Si1-H) is a covalent bond. The optimized Si1–NH_2 bond length in LM2 is 1.752 Å, in good agreement with the XPD experimental value of 1.73 ± 0.08 Å.[15]

The process from LM2 to LM3 (:Si1 ··· NH_2–Si1H) corresponds to NH_2 insertion into the surface Si1–Si1 dimer bond. Similarly to the process of recombination-desorption from LM2 to LM1/R1, the insertion process from LM2 to LM3 is endergonic, being characterized by a large activation barrier of about 46 kcal mol^{-1} and an endothermicity of 21.7 kcal mol^{-1}. This finding agrees well with the experimental observation that NH_2(a) attaches to the surface and is stable up to more than 600 K.[8–15]

LM3 tends to transfer one H from its amino group to :Si1. LM4 (H-Si1-NH-Si1-H) thus formed is thermodynamically more stable than LM3, as every Si is tetrahedrally coordinated in LM4. A moderate activation energy, 32.1 kcal mol^{-1}, is required from LM3 (:Si1 ··· NH_2–Si1H) to TS3, followed by a large exothermicity of −65.7 kcal mol^{-1} from TS3 to LM4.

The process from LM4 (H-Si1-NH-Si1-H) to P1 (HSi1-N=Sil) involves the liberation of H_2(g). Experimentally, liberation of H_2(g) was observed around 800 K.[8–15] Our calculation shows a large activation barrier of 70.7 kcal mol^{-1} for this process. The optimized HSi1–N(a) bond length in P1 is 1.706 Å shorter than a normal Si–N single bond length (1.75 Å). The optimized Si1=N (f) bond length in P1 is 1.610 Å; this shows clearly the character of a Si=N double bond. The overall process from R1 to P1 has an apparent activation energy of 5.7 kcal mol^{-1}. At lower coverage, it is very likely for H(a) to diffuse to a neighboring dimer so as to facilitate the formation of P1. (See sections 3 and 4.)

Figure 2 shows two other pathways that can lead to the formation of P1 (HSi1-N=Si1). Starting from LM3 (:Si1 ··· NH_2–Si1H), instead of transferring one H to :Si1 to make LM4 (H-Si1-NH-Si1-H), it might be possible to liberate a H_2 to make LM5 (•Si1-NH-Si1•). Relative to LM4, LM5 is less stable by 54.0 kcal mol^{-1}. This can be understood by the fact that the energy gain of making a H–H bond (D°_{298}(H–H) = 104.2 kcal mol^{-1}[40]) could not compensate for the energy loss of breaking two Si–H bonds (e.g. D°_{298}(H–SiH3) = 91.8 kcal mol^{-1}[40]). LM5 is connected to P1 (HSi1-N=Si1) via TS6, at which H moves from N to Si1. The calculated

  0947-6539/02/0823-5353 $ 20.00+.50/0

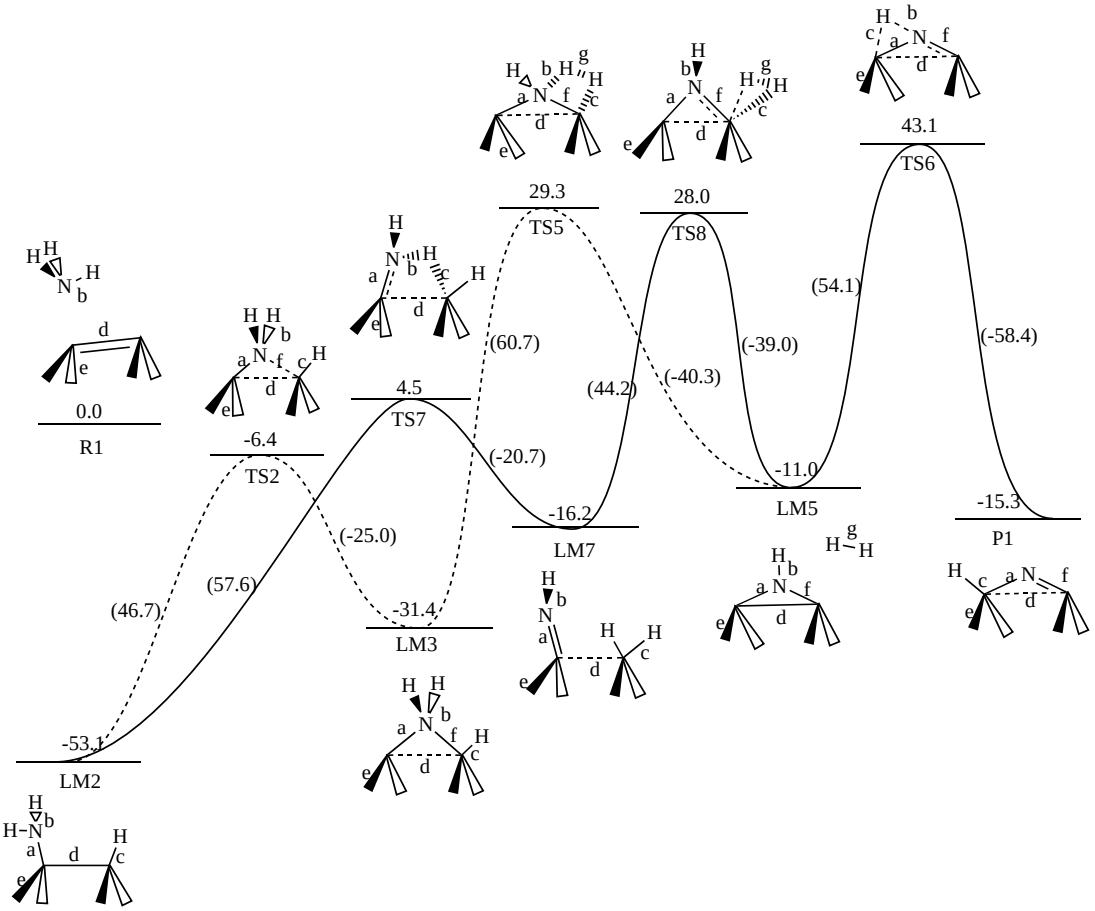

Figure 2. Mechanisms for the formation of surface product P1 (HSi1-N=Si1). These pathways differ from the mechanism in Figure 1 by the formation of the LM7 dihydride species and/or LM5 (Si1-NH-Si1). These mechanisms are less plausible than that in Figure 1.

barrier heights from LM3 to LM5 and LM5 to P1 are 60.7 and 54.1 kcal mol^{-1}, respectively.

Another route shown in Figure 2 involves the formation of LM7 (HN=Si1 + H–Si1-H) as an intermediate. We find a transition state, TS7, that connects LM2 to LM7. Instead of NH_2 insertion, TS7 involves N–H bond cleavage. LM7 has a dihydride-like structure, which has been postulated as an intermediate involved in the H_2 desorption.[41, 42] We calculate that the activation barrier to liberating H_2 from LM7 is 44.2 kcal mol^{-1}, leading to the formation of LM5 (·Si1-NH-Si1·).

The pathways shown in Figure 2 have a net activation barrier of 43.1 kcal mol^{-1} from R1 to P1. Thus P1 cannot be made through these pathways.

2. Formation of subsurface N(a): $(Si2)_2$-N-Si1H_2-Si1H (P2): Figure 3 summarizes the reaction pathway for the formation of the subsurface N(a). Instead of attacking the surface Si1–Si1 dimer bond, the NH_2 in LM2 (NH_2-Si1-Si1-H) attacks a subsurface, Si2. The process from LM2 (Si2, NH_2-Si1-Si1-H) to LM9 (Si2-NH_2···:Si1–Si1H) is an analogy to the process from LM2 to LM3 (:Si1 ··· NH_2–Si1H) in Figure 1. Although it is generally believed that the Si1–Si1 dimer bond is the weakest of all the bonds, our calculations indicate that the energy cost for the insertion of NH_2 into a Si1–Si2 backbond could be comparable to that into a Si1–Si1 dimer bond. TS9 is 5.2 kcal mol^{-1} below the vacuum level; this suggests that there should be a certain probability for the formation of LM9.

The exothermicity from R1 to LM9 is calculated to be -30.4 kcal mol^{-1}. In LM9 (Si2-NH_2···:Si1–Si1H), NH_2 is covalently bound to the subsurface Si2 with a Si2–NH_2 bond length (f) of 1.852 Å; NH_2 is datively bound to the surface Si1 with a long Si1–NH_2 bond length (a) of 2.108 Å. It can be visualized that a lone pair of electrons is located at Si1, ready to donate electrons to the anti-bonding orbital of N–H so as to break an N–H bond. Similarly to the process from LM3 (:Si1 ·· ·· NH_2–Si1H) to LM4 (HSi1-NH–Si1H) in Figure 1, the activation barrier for the decomposition process from LM9 (Si2-NH_2···:Si1–Si1H) to LM10 (Si2-NH-Si1H-Si1H) is found to be 31.0 kcal mol^{-1}. This may correspond to the experimental activation energy of 30 ± 4 kcal mol^{-1} for the decomposition of NH_2(a) based on the decreasing of the $SiNH_2^+$ SSIMS signal.[14] The resultant LM10 has an imino group (NH) bridging Si1 and Si2 with a Si1–NH bond length (a) of 1.761 Å and Si2–NH bond length (f) of 1.754 Å. LM10 (Si2-NH-Si1H-Si1H) is 11.1 kcal mol^{-1} more stable than LM2 (NH_2-Si1-Si1-H).

As long as the barriers to TS9 and TS10 could be overcome, it might be relatively easier for the reaction to proceed up to the complete dissociation of NH_3 and the formation of subsurface N(a) (See Figure 3). We find that the imino group can rearrange from a state of bridging one surface Si1 and one

0947-6539/02/0823-5354 $ 20.00+.50/0 *Chem. Eur. J.* **2002**, *8*, No. 23

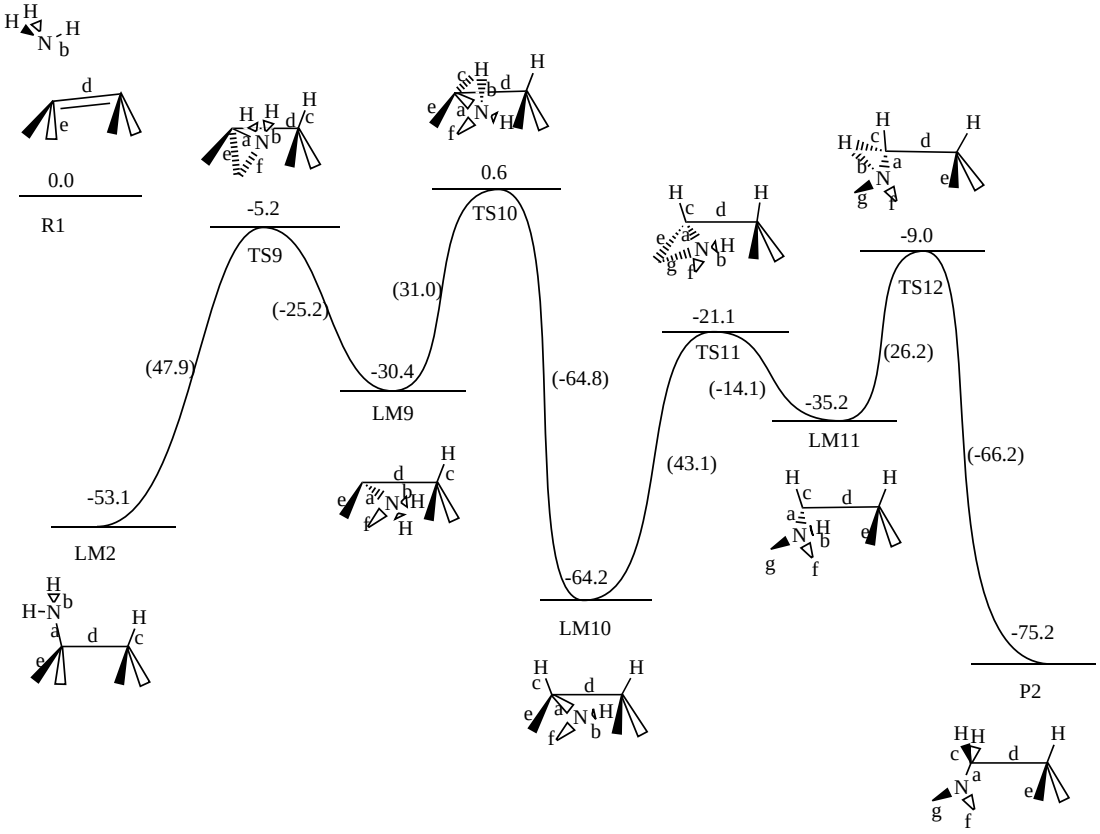

Figure 3. Mechanism for the formation of subsurface product P2 ($(Si2)_2$-N-$Si1H_2$-Si1-H). They key step is NH_2 insertion into the Si1–Si2 backbond.

subsurface Si2, such as in LM10, to a state of bridging two subsurface Si2s (see LM11 in Figure 3). The activation barrier to this rearrangement is found to be 43.1 kcal mol^{-1}. The structure of LM11 facilitates the final cleavage of the last N–H bond and the formation of the Si1–H bond. In P2 ($(Si2)_2$-N-$Si1H_2$-Si1H), N binds to two subsurface Si2s and one surface Si1 in a nearly planar geometry with three equivalent Si–N bonds (a, g, and f at 1.771 Å). This is in good agreement with HREELS deductions at 900 K, in which 45 and 100 meV losses were attributed to the symmetric-breathing mode and the asymmetric in-plane bond-stretching mode of the nearly planar Si_3N species.[10]

Figure 4 illustrates the possible pathways for the H_2 liberation from P2. H_2 desorption can occur either from the dihydride on the same Si1 atom (TS13, TS16), or across two different Si1 atoms (TS14). H_2 desorption can be a one-step process (TS13 or TS14) or a two-step process (TS15 and TS16). We find that the most feasible pathway is the one-step process for H_2 liberation over the same Si1 atoms (TS13). The calculated activation barrier from P2 ($(Si2)_2$-N-$Si1H_2$-Si1H) to LM13 ($(Si2)_2$-N-Si1-Si1H) via TS13 is 53.9 kcal mol^{-1}.

It is worth pointing out that TS15 is a transition state that corresponds to an intradimer hydrogen diffusion. Our calculated value of 45.6 kcal mol^{-1} is in good agreement with the data in literature. Nachtigall and Jordan reported a barrier of 42.9 kcal mol^{-1} for the intradimer hydrogen diffusion; while Wu and Carter obtained a barrier of 45.8 kcal mol^{-1} for the intrarow hydrogen diffusion.[41, 42]

3. NH_2(a) insertion in the absence of neighboring H(a): Except for an early study in which NH_3 decomposition over adjacent Si–Si dimer rows was postulated,[19] most research seems to favor a picture that the initial NH_3 decomposition occurs within a single dimer.[20–27] LM17 (NH_2-Si1-Si1$^{\bullet}$) in Figure 5 could be a product of NH_3 decomposition over two neighboring dimers. It could also be a resultant for H(a) in LM2 (NH_2-Si1-Si1-H) to diffuse over to another dimer. Although this diffusion barrier is not calculated rigorously in this work, we tentatively adopt the value of 45.6 kcal mol^{-1}, discussed in the previous section. Depending on the diffusion pathway and the local environment, the real diffusion barrier could be lower or higher.[41–48]

LM17 is unstable by 6.3 kcal mol^{-1} relative to LM2. This is understandable, as an extra Si1–Si1 π bond is broken in forming LM17. In fact, based on the kinetic data of isothermal measurements, Höfer et al. deduced a value of 5.8 kcal mol^{-1} for the Si–Si π-bonding interaction.[43]

It would be interesting to examine the spin-density change along the pathway shown in Figure 5. It is found that 0.80 spin density is located on the right Si1 of LM17 (NH_2-Si1-Si1$^{\bullet}$). As NH_2(a) is inserted into Si1–Si1, we get LM18. Although we denote LM18 as (:Si1 $\cdots$ NH_2–Si1$^{\bullet}$), spin density is more or less spread over the two surface Si1s. The right-hand Si1 possesses a spin density of 0.60, and the corresponding Si1-NH_2 bond length (f) is 1.844 Å; while the left-hand Si1 possesses a spin density of 0.20, and the corresponding Si1-NH_2 length (a) is 2.169 Å. LM19 (H-Si1-NH-Si1$^{\bullet}$) is an imino (NH) adsorption mode whose spin density is mainly localized

  0947-6539/02/0823-5355 $ 20.00+.50/0

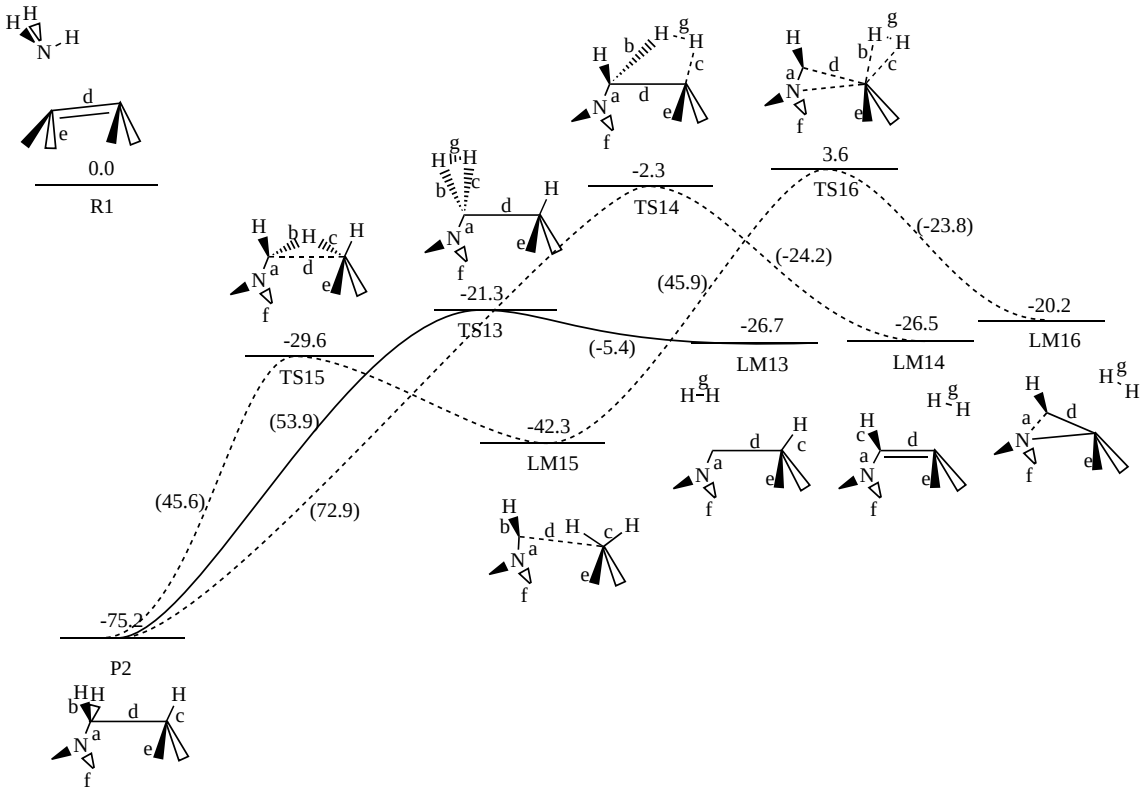

Figure 4. Mechanisms for hydrogen diffusion (TS15) and H_2 liberation from P2 ($(Si2)_2$-N-$Si1H_2$-Si1-H).

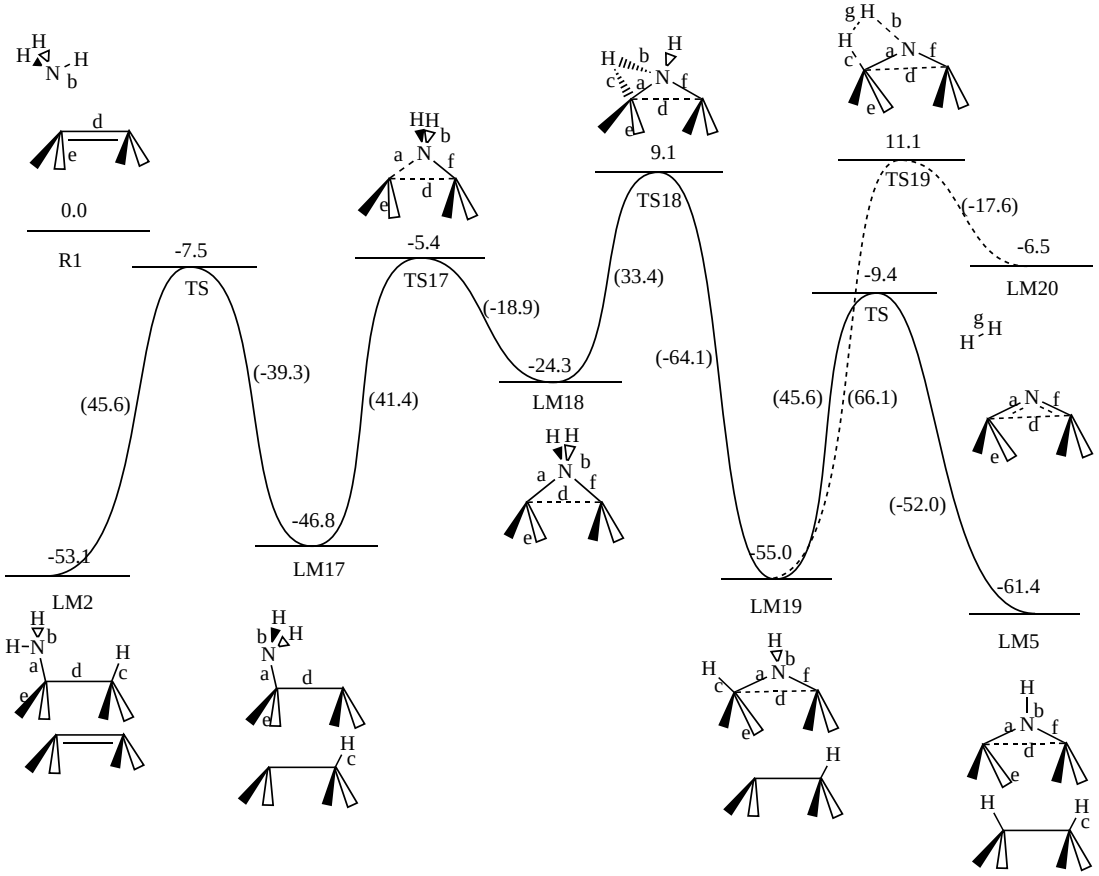

Figure 5. Mechanisms for the formation of the surface products LM20 (Si1-N-Si1) and LM5 (Si1-NH-Si1). The effect of hydrogen diffusion is investigated. The process from R1 to LM20 is analogous to Figure 1 from R1 to P1, but is less favorable. Hydrogen diffusion greatly stabilizes LM5 as compared with the mechanism in Figure 2.

0947-6539/02/0823-5356 $ 20.00+.50/0 *Chem. Eur. J.* **2002**, *8*, No. 23

on the right-hand Si1. As opposed to the nearly planar configuration in LM4 (H-Si1-NH-Si1-H) or LM5 (•Si1-NH-Si1•), it is interesting to see that the N in LM19 (H-Si1-NH-Si1•) is in a trigonal pyramidal geometry. After H_2 liberation from LM19, the product is LM20 (•Si1-N-Si1•). One might expect that the Si1–Si1 dimer bond is restored and spin is localized at N in LM20. However, we find the Si1–Si1 separation (d) is about 3.230 Å and the spin density is quite spread. There is 0.59 spin density on the left-hand Si1, whose Si1-N bond length (a) is 1.633 Å. There is 0.36 spin density on the right Si1, whose Si1-N bond length (f) is 1.671 Å (c.f. Figure 5 and Table S5 in the Supporting Information). Clearly, the bonding of the Si1-N-Si1 unit in LM20 should be best viewed as a $_3{}^3$, such that every Si–N gains certain double-bond character.

The overall process shown in Figure 5 is similar to that in Figure 1. The barrier heights for NH_2(a) insertion (LM17 → TS17) and H_2 liberation (LM19 → TS19) are 41.4 and 66.1 kcal mol^{-1}, respectively, and are smaller than the corresponding barrier heights (NH_2 insertion LM2 → TS2: 46.7 and H_2 liberation LM4 → TS4: 70.7 kcal mol^{-1}) shown in Figure 1 when the neighboring H(a) is present. However, the corresponding local minima (LM17, LM18, LM19, and LM20) in the potential-energy surface are all less stable than their counterparts (LM2, LM3, LM4, and P1). The net activation barrier for this route from R1 to LM20 is 11.1 kcal mol^{-1}. We therefore conclude that diffusion of H(a) does not help the NH_3 decomposition in a way shown in Figure 5.

It is interesting to relate LM19 to LM5 by hydrogen diffusion. By comparing Figures 2 and 5, we note that hydrogen diffusion greatly stabilizes the formation of LM5. Instead of forming LM5 + H_2 as in Figure 2, LM5 + H-Si1-Si1-H are formed in Figure 5. The mechanism shown in Figure 5 brings LM5 formation -61.4 kcal mol^{-1} below the entrance level (R1), which in turn should facilitate the formation of product P1.

Figure 6 shows that how H(a) diffusion will affect the NH_2(a) insertion into the Si1–Si2 backbond. TS21 is 10.7 kcal mol^{-1} below the entrance level (R1) and 5.5 kcal mol^{-1} lower in energy than TS9 (Figure 3). The insertion barrier from LM17 (Si2, NH_2-Si1-Si1•) to TS21 is significantly (11.8 kcal mol^{-1}) lower than that from LM2 (Si2, NH_2-Si1-Si1-H) to TS9. However, the exothermicity from TS21 to LM21 (Si2-NH_2···:Si1-Si1•) is only -13.8 kcal mol^{-1}, 11.4 kcal mol^{-1} smaller than that from TS9 to LM9 (Si2-NH_2···:Si1-Si1H). This makes LM21 5.9 kcal mol^{-1} unstable with respect to LM9. This may be understandable as the spin density spreads more or less over two Si1 atoms. Although the activation barrier for H transfer from LM21 to TS22 is the same as that from LM9 to TS10, TS22 is 6.1 kcal mol^{-1} higher in energy than its counterpart TS10 (Figure 3). Indeed, this ~6 kcal mol^{-1} energy difference has been carried over through the whole decomposition process from LM21 (Si2, Si2-NH_2···:Si1–Si1•) to LM24 ((Si2)2-N-Si1H_2-Si1•), as shown in Figure 6, making the decomposition process less favorable than that of Figure 3. We therefore conclude that although H(a) diffusion helps the NH_2(a) insertion into the Si1–Si2 backbond by lowering the insertion barrier, the net decomposition process becomes less favorable as the decomposition potential-energy surface is raised by ~6 kcal mol^{-1} owing to the delocalization of the spin density.

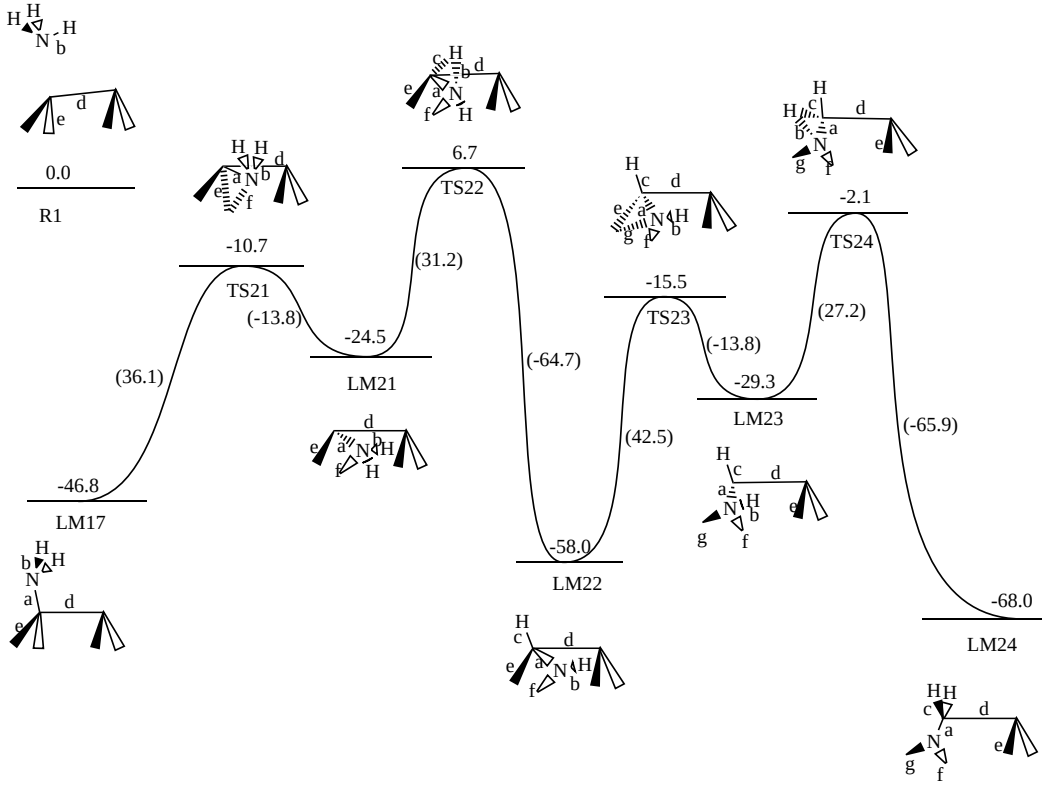

Figure 6. Mechanism for the formation of subsurface product LM24 ((Si2)$_2$-N-Si1H_2-Si1), in analogy to the mechanism in Figure 3. A dangling bond helps to reduce the NH_2-insertion barrier, but destabilizes the insertion products. The whole process (R1 → LM24) is less favorable than that (R1 → P2) shown in Figure 3.

  0947-6539/02/0823-5357 $ 20.00+.50/0

4. NH_2(a) decomposition in the absence of neighboring H(a): Besides NH_2(a) insertion into the Si1−Si1 dimer bond, shown in Figure 5, NH_2(a) can undergo N−H decomposition, as shown in Figure 7. This process, from LM17 (NH_2-Si1-Si1•) to P1 (H-Si1-N=Si1), has one-to-one correspondence to the process from LM1 (NH_3 ··· Si1−Si1:) to P1. LM1 (Figure 1) is a coordination complex that is characterized by a dative bond between NH_3 and Si1. The Si1−N bond length (a) in LM1 is 2.014 Å. On the other hand, LM17 is a covalent complex with a Si1−NH_2 bond length (a) of 1.750 Å. Therefore, LM17 is $46.8 - 21.6 = 25.2$ kcal mol^{-1} more stable than LM1. However, as a result of dipole polarization, charge density is localized on the right-hand Si1 in LM1, ready for the decomposition of the N−H bond. This mechanism does not operate in LM17. Therefore, the activation barrier to decomposition of an N−H bond on going from LM17 (NH_2-Si1-Si1•) to TS25 is $48.1 - 14.2 = 23.9$ kcal mol^{-1} higher than that from LM1 (NH_3 ··· Si1−Si1:) to TS1. The net result is that TS25 is 1.3 kcal mol^{-1} above the entrance channel (R1), whereas TS1 is -7.4 kcal mol^{-1} below R1. The resultant LM25 (•NH-Si1-Si1-H) is $-25.9 + 53.1 = 27.2$ kcal mol^{-1} less stable than LM2 (NH_2-Si1-Si1-H), as there is no free valency in LM2. The radical nature of LM25 makes NH insertion 8much easier than NH_2 insertion (10.9 vs. 46.7 kcal mol^{-1}). It is anticipated that LM26 (•Si1-NH-Si1-H) is more stable than LM3 (:Si1 ··· NH_2−Si1H), and that the process from LM26 (•Si1-NH-Si1-H) to LM27 (H-Si1-N-Si1-H) is less feasible than from LM3 (:Si1 ··· NH_2−Si1H) to LM4 (H-Si1-NH-Si1-H) (Figure 1). As in Figure 4 for the process from P2 to TS15, we assign a H diffusion barrier of 45.6 kcal mol^{-1} from LM27 to make P1 (H-Si1-N=Si1). Recall that the H_2 liberation barrier from LM4 (H-Si1-NH-Si1-H) to P1 (H-Si1-N=Si1) is 70.7 kcal mol^{-1}. Comparison of the mechanisms shown in Figures 1 and 7 suggests that H diffusion to vacate the neighboring Si1 site should facilitate the formation of P1 (H-Si1-N=Si1).

Instead of NH insertion into the Si1−Si1 dimer bond, as is shown in Figure 7 from LM25 (•NH-Si1-Si1-H) to LM26 (•Si1-NH-Si1-H), NH insertion into the Si1−Si2 backbond is also possible. This will lead to the formation of subsurface N(a), going through pathways similar to those shown in Figures 3 and 6. As is shown above, it is easier to insert NH than to insert NH_2. The barrier height for the process from LM25 (Si2, •NH-Si1-Si1-H) to LM28 (Si2-NH-Si1-Si1H) is only 9.2 kcal mol^{-1} (Figure 8), significantly smaller than those from LM2 (Si2, NH_2-Si1-Si1-H) to LM9 (Si2-NH_2 ··· :Si1−Si1H) at 47.9 kcal mol^{-1} (Figure 3) and from LM17 (Si2, NH_2-Si1-Si1•) to LM21 (Si2-NH_2 ··· :Si1−Si1•) at 36.1 kcal mol^{-1} (Figure 6). The stability of the insertion products follows the order that

	ΔH_{298} [kcal mol^{-1}]
LM28 (Si2-NH-Si1-Si1H)	− 50.8
> LM9 (Si2-NH_2 ··· :Si1−Si1H)	− 30.4
> LM21 (Si2-NH_2 ··· :Si1−Si1•)	− 24.5

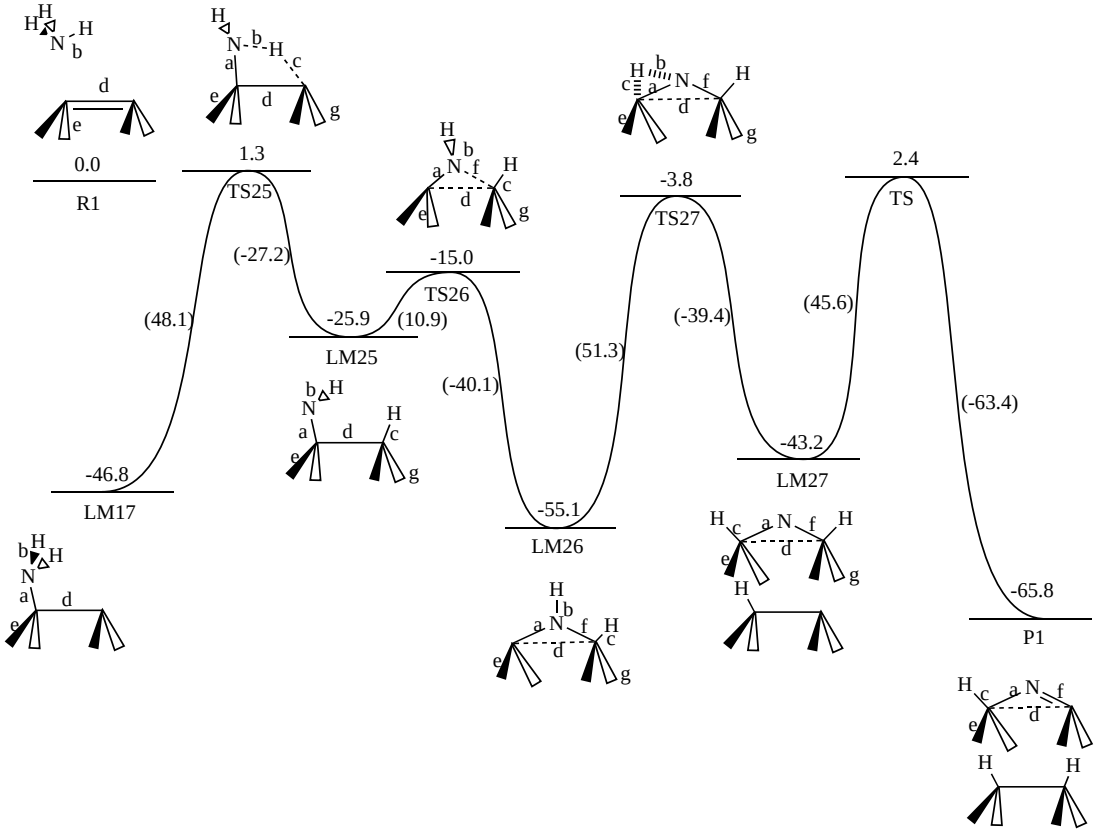

Figure 7. Mechanism for the formation of surface products LM27 (H-Si1-N-Si1-H) and P1 (H-Si1-N=Si1), in analogy to the mechanism in Figure 1. The key steps are hydrogen diffusion as well as •NH insertion into the surface Si1−Si1 dimer bond.

0947-6539/02/0823-5358 $ 20.00+.50/0 *Chem. Eur. J.* **2002**, *8*, No. 23

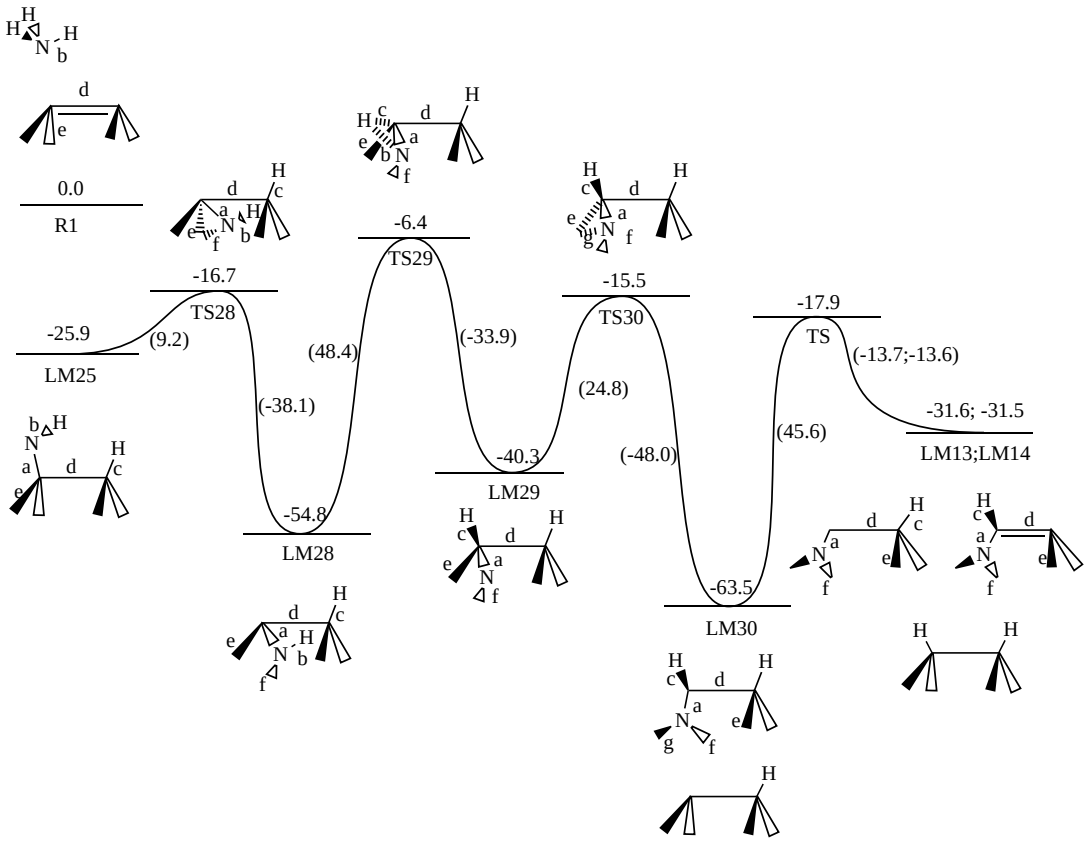

Figure 8. Mechanism for the formation of subsurface product LM30 ($(Si2)_2$-N-Si1H-Si1H), in analogy to the mechanism in Figure 3. The key steps are hydrogen diffusion and ·NH insertion into the Si1–Si2 backbond.

Thus the barrier for the subsequent H transfer from N to Si1 from LM28 (Si2-NH-Si1-Si1H) to LM29 (Si2-N-Si1H-Si1H) via TS29 is significantly higher at 17.4 kcal mol^{-1} than those from LM9 to LM10 via TS10 and from LM21 to LM22 via TS22. However, owing to the strong exothermicity of the formation LM28 (Si2-NH-Si1-Si1H), TS29 is still -6.4 kcal mol^{-1} below the vacuum level (R1), whereas TS10 and TS22 are 0.6 and 6.7 kcal mol^{-1}, respectively, above the vacuum level. The following N attack on the subsurface Si2 (from LM29 to LM30 in Figure 8) is much easier (17.7 kcal mol^{-1}) than the corresponding process of NH attacking the subsurface Si2 from LM22 to LM23 in Figure 6 and from LM10 to LM11 in Figure 3. Hence our calculation results show that H diffusion to vacate the neighboring Si1 site can help the formation of subsurface Si_3–N in a way shown in Figure 8.

Discussion

Three elementary processes have been studied in the present work, that is, N–H bond cleavage, NH_x ($x = 1-2$) insertion, and H_2 liberation. Table 1 summarizes the activation barriers of all the possible ways of N–H decomposition studied here. As the strength of an N–H bond follows the order that NH_2–H (108.2 kcal mol^{-1}) > NH–H (91.9) > N-H (81.0),[40] it would be expected that the feasibility of a reaction to break an N–H bond follows the reverse order of the N–H bond strength. This is not at all the case. Our calculations reveal that the feasibility of an N–H bond-decomposition reaction is closely related to the availability and the localization of a lone pair of electrons on the Si, where a new Si–H bond is going to form. We find that N–H decomposition barriers range from 14.2 to 57.6 kcal mol^{-1}. The lowest barrier occurs at the first NH_2–H bond decomposition (LM1 → LM2, see Figure 1). The lone pair of NH_3 polarizes the electron of the Si1=Si1 dimer bond. In LM1 (NH_3···Si1–Si1:), the dimer bond buckles up with a pair of electrons well localized at the other end of Si1. This kind of geometric and electronic structure greatly facilitates the NH_2–H bond decomposition.

On the other hand, we find the highest barrier occurs at LM2 → LM7 (see Figure 2). The NH–H bond is decomposed over the other Si1, which is already tetrahedrally coordinated. The second highest barrier occurs at LM5 → P1, in which the N–H bond is decomposed over the Si1 radical, rather than the Si1 lone pair.

Table 2 summarizes the NH_x insertion barriers. We find that:

1) Barriers for NH_x insertion into the Si1–Si2 backbond are similar to that into the Si1–Si1 dimer bond. Thus E_a for LM2 (Si2, NH_2-Si1-Si1-H) → LM9 (Si2-NH_2···:Si1–Si1H) at 47.9 kcal mol^{-1} is similar to that for LM2 (NH_2-Si1-Si1-H) → LM3 (:Si1···NH_2–Si1H) at 46.7 kcal mol^{-1}.
2) Dangling bonds help the NH_x insertion. Thus E_a for LM17 (Si2, NH_2-Si1-Si1·) → LM21 (Si2-NH_2···:Si1–Si1·) is 11.8 kcal mol^{-1} smaller than the analogous process LM2 → LM9 in the presence of H(a).

  0947-6539/02/0823-5359 $ 20.00+.50/0

Table 2. NH_x insertion barrier [kcal mol^{-1}].

Reactions	Figure		E_a
LM2 → LM9	3	(Si2, NH_2-Si1-Si1H) → (Si2-NH_2 ··· :Si1-Si1H)	47.9
LM2 → LM3	1	(NH_2-Si1-Si1-H) → (:Si1 ··· NH_2–Si1H)	46.7
LM10 → LM11	3	(Si2, Si2-NH-Si1H-Si1H) → ($(Si2)_2$-NH ··· :Si1H–Si1H)	43.1
LM22 → LM23	6	(Si2, Si2-NH-Si1H-Si1•) → ($(Si2)_2$-NH ··· :Si1H–Si1•)	42.5
LM17 → LM18	5	(NH_2-Si1-Si1•) → (:Si1 ··· NH_2–Si1•)	41.4
LM29 → LM30	8	(Si2, Si2-N-Si1H-Si1H) → ($(Si2)_2$-N-Si1H-Si1H)	24.8
LM17 → LM21	6	(Si2, NH_2-Si1-Si1•) → (Si2-NH_2 ··· :Si1–Si1•)	36.1
LM25 → LM26	7	(•NH-Si1-Si1-H) → (•Si1-NH-Si1-H)	10.9
LM25 → LM28	8	(Si2, •NH-Si1-Si1-H) → (Si2-NH-Si1-Si1H)	9.2

3) •NH-radical insertion is much easier than NH_2 insertion. Thus E_a for LM25 (Si2, •NH-Si1-Si1-H) → LM28 (Si2-NH-Si1-Si1H) is only 9.2 kcal mol^{-1}, significantly (38.7 kcal mol^{-1}) smaller than the counterpart process LM2 → LM9.

Table 3 summarizes the hydrogen-diffusion and H_2-liberation barriers. P2 ($(Si2)_2$-N-Si1H_2-Si1H) → LM15 ($(Si2)_2$-N-Si1H, H-Si1-H) represents the process for the intradimer hydrogen diffusion. There have been several guesses as to the barrier to this process, ranging from 41.5[44] to 57.7 kcal mol^{-1}.[45] It was concluded that barriers increase in magnitude in the following fashion:[45] diffusion between dimers in the same dimer row (46.1 kcal mol^{-1}), diffusion between dangling bonds on the same dimer (57.7 kcal mol^{-1}), and diffusion between neighboring dimers in adjacent rows (62.3 kcal mol^{-1}). We obtained a intradimer hydrogen-diffusion barrier of 45.6 kcal mol^{-1}. We expect that the barrier for an intrarow hydrogen diffusion should be lower and should also work in the nitridation process.

Table 3. Hydrogen diffusion and desorption barrier [kcal mol^{-1}].

Reactions	Figure		E_a
LM7 → LM5	2	(H-N=Si1, H-Si1-H) → (•Si1-NH-Si1•) + H_2	44.2
P2 → LM15	4	($(Si2)_2$-N-Si1H_2-Si1H) → ($(Si2)_2$-N-Si1H, H-Si1-H)	45.6
LM15 → LM16	4	($(Si2)_2$-N-Si1H, H-Si1-H) → ($(Si2)_2$-N-Si1-Si1H) + H_2	45.9
P2 → LM13	4	($(Si2)_2$-N-Si1H_2-Si1H) → ($(Si2)_2$-N-Si1-Si1H) + H_2	53.9
LM3 → LM5	2	(:Si1 ··· NH_2–Si1H) → (•Si1-NH-Si1•) + H_2	60.7
LM19 → LM20	5	(H-Si1-NH-Si1•) → (•Si1-N-Si1•) + H_2	66.1
LM4 → P1	1	(H-Si1-NH-Si1-H) → (HSi1-N=Si1) + H_2	70.7
P2 → LM14	4	($(Si2)_2$-N-Si1H_2-Si1H) → ($(Si2)_2$-N-Si1H=Si1) + H_2	72.9

Depending on the local environment, we find that the H_2 liberation barriers vary from 44.2 to 72.9 kcal mol^{-1}. The lowest barrier occurs at LM7 (H-N=Si1, H-Si1-H) → LM5 (•Si1-NH-Si1•) + H_2. This corresponds to H_2 liberation from an isolated dihydride. It was claimed that this isolated-dihydride mechanism was the only mechanism that provided a dynamically and kinetically consistent explanation for the H_2 desorption from Si(100)-(2 × 1).[45] Experimentally, the H_2 liberation barriers were determined to be 45.0 ± 2.3 – 66.0 ± 4.6 kcal mol^{-1}.[43, 46–48] Recent work by Zimmermann,[49] Heinz,[50] and Höfer[51] has shown that the lowest pathway involves two dimers, a mechanism that cannot be addressed in the present single-dimer model.

The mechanisms for the complete decomposition of NH_3 explored here are summarized in Figure 9.

Reaction from R1 to LM2 represents the facile initial decomposition of NH_3 over the surface Si dimer to produce NH_2(a) and H(a). There exist large barriers to prevent NH_2(a) from undergoing further decomposition to N(a) or

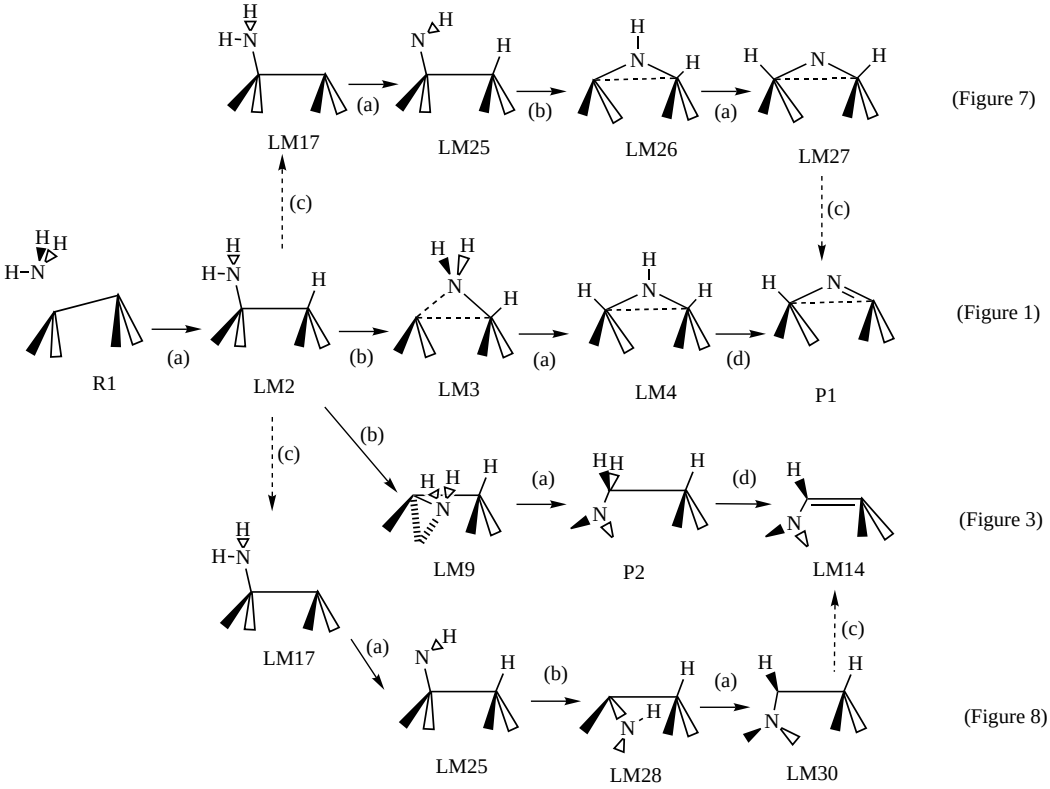

Figure 9. Summary of the mechanisms for the complete decomposition of NH_3. a) NH_x–H bond decomposition, b) NH_x insertion, c) H diffusion, and d) H_2 liberation.

0947-6539/02/0823-5360 $ 20.00+.50/0 *Chem. Eur. J.* **2002**, *8*, No. 23

recombination–desorption to $NH_3(g)$. The reverse barriers from LM2 to LM1 is calculated to be 45.7 kcal mol^{-1} (Figure 1), which is comparable to the barriers for $NH_2(a)$ insertion into the Si1–Si1 dimer bond (LM2 → LM3, 46.7 kcal mol^{-1}) or $NH_2(a)$ insertion into the Si1–Si2 backbond (LM2 → LM9, 47.9 kcal mol^{-1}).

This clearly explains the experimental observation that $NH_2(a)$ is stable up to more than 600 K.[8–15] The comparable barriers for $NH_2(a)$ + H(a) recombination and the further decomposition of $NH_2(a)$ suggest that both mechanisms are operating. A subtle change of the experimental condition would make one process outweigh the other. In fact, based on the H_2-desorption yield, Chen et al. concluded that recombination–desorption to $NH_3(g)$ is the main channel and that complete decomposition to N(a) is a minor channel.[12] We find the surface N(a) (P1) formation (see Figure 1) has a net barrier of 5.7 kcal mol^{-1}, characterized by a huge (70.7 kcal mol^{-1}) barrier of H_2 liberation if neighboring dimer bonds have been passivated.

On the other hand, since the N/Si AES ratio showed negligible change in the temperature range 600–700 K, Dress et al. concluded that dissociation is the main channel and recombination–desorption is a minor channel.[13] The subsurface N(a) (P2) formation (shown in Figure 3) may fit more into this observation. The apparent activation barrier for the formation of Si_3N is calculated to be only 0.6 kcal mol^{-1}. Experimentally, although most $NH_2(a)$ species were found to be stable up to 630 K and to decompose rapidly between 630 and 730 K, slow thermal decomposition of $NH_2(a)$ was observed to start at 320 K.[14]

It is interesting to notice that the dissociation of NH_3 on Si(100) via a pathway of NH_2 insertion into the Si1–Si2 backbond will preserve the (2×1) local symmetry, in agreement with the low-energy electron diffraction and STM observations[6, 13] that the chemisorbed Hs saturate the surface dangling bonds while nitrogens occupy the subsurface sites.

We find hydrogen diffusion possesses a similar activation barrier of 45.6 kcal mol^{-1} to the $NH_2(a)$ insertion or $NH_2(a)$ + H(a) recombination. Therefore, at the same temperature at which insertion or recombination occurs, hydrogen diffusion should also be in effect. The mechanisms represented in Figures 7 and 8 show that hydrogen diffusion to free the neighboring dangling bond will facilitate the formation of P1 and P2.

It should be emphasized that P1 has a surface Si=N unit, similar to the terminal Si=N_t pair in silicon nitride Si_3N_4;[52] while P2 possesses a near-planar subsurface unit Si_3N, in analogy to a central nitrogen atom (N_c) bound to three silicon atoms in the Si_3N_4 environment.[52] The Si=N pair in P1 has two dangling bonds, similar to those on the $Si(100)-(2 \times 1)$ surface. Thus, the reactions summarized in Figure 9 can be repeated, leading to the growth of silicon nitride film:

$$NH_3 + P1\ (HSi1\text{-}N{=}Si1) \cdots\rightarrow (HSi1\text{-}NH\text{-}Si1\text{-}NH_2)$$

$$(HSi1\text{-}NH\text{-}Si1\text{-}NH_2, 2Si2) \cdots\rightarrow (HSi1\text{-}NH\text{-}H_2Si1\text{-}N\text{-}(Si2)_2)$$

$$(HSi1\text{-}NH\text{-}H_2Si1\text{-}N\text{-}(Si2)_2) \cdots\rightarrow (Si1{=}N_t\text{-}Si1\text{-}N_c\text{-}(Si2)_2) + 2H_2$$

High temperatures are necessary to facilitate the $NH_2(a)$ insertion and to desorb hydrogen so as to produce surface dangling bonds and restore surface reactivity. Experimentally, it is found that an electron beam is so effective in removing hydrogen from $NH_x(a)$ and from the silicon surface that the nitridation of $Si(100)-(2 \times 1)$ by NH_3 can occur at temperatures as low as 90 K.[7, 53]

Conclusion

Hybrid density functional theory (B3LYP) has been used to explore the adsorption and decomposition of NH_3 on the $Si(100)-(2 \times 1)$ surface. N–H bond-cleavage, NH_x insertion into the Si–Si dimer bond or backbond, hydrogen-diffusion, and H_2-liberation processes have been investigated. The main results are summarized as follows:

1) $NH_3(g)$ adsorbs molecularly onto $Si(100)-(2 \times 1)$ with an adsorption energy of 21.6 kcal mol^{-1}. $NH_3(a)$ dissociates to $NH_2(a)$ and H(a) with an activation energy of 14.2 kcal mol^{-1} and reaction exothermicity of -45.7 kcal mol^{-1}. Thus the dissociation of NH_3 follows a trapping-mediated mechanism. This process is below the vacuum level, it therefore can happen at low temperature.
2) The resultant $NH_2(a)$ and H(a) are tied to the surfaces. Either $NH_2(a)$ + H(a) recombination, $NH_2(a)$ insertion into the Si1–Si1 dimer bond or the Si1–Si2 backbond, or H(a) diffusion needs to overcome a large and similar amount of activation barrier ($\sim$46 kcal mol^{-1}). Thus, these processes will compete with each other when the surface temperature is increased. Different reaction conditions would favor one process over the others.
3) The N–H decomposition barrier is found to range from 14.2 to 57.6 kcal mol^{-1}. The feasibility of an N–H bond cleavage does not follow the reverse order of N–H bond strength. Instead, it is closely related to the activity of the Si atoms. The lowest barrier occurs at the first NH_2–H bond decomposition (see Figure 1); while the highest barrier occurs at the NH–H bond decomposition to a tetrahedrally coordinated Si1 (see Figure 2).
4) We find that the NH_x insertion barrier is within the range of 9.2 to 47.9 kcal mol^{-1}. The ·NH-radical insertion is much easier than the NH_2 insertion. Hydrogen diffusion to vacate the neighboring Si1 site can help to reduce the NH_x-insertion barrier. The lowest barrier is for the ·NH radical insertion into the backbond; while the NH_2 insertion into the backbond is the most difficult.
5) The H_2 liberation barrier is found to range from 44.2 to 72.9 kcal mol^{-1}. H_2 liberation from an isolated dihydride is easiest; while that across two different Si1 atoms is most difficult.
6) We find that NH_2 insertion into the surface Si1–Si1 dimer leads to the formation of a surface Si=N unit, similar to the terminal Si=N_t pair in Si_3N_4; while the NH_2 insertion into the Si1–Si2 backbond leads to the formation of a near-planar subsurface Si_3N, in analogy to a central nitrogen atom bounded to three silicon atoms in a Si_3N_4 environment. Based on these results, a plausible mechanism for the nitridation of $Si(100)-(2 \times 1)$ by NH_3 is proposed.

  0947-6539/02/0823-5361 $ 20.00+.50/0

These results can be used as the quantum-mechanical input for a chemical-kinetics model of chemical-vapor deposition (CVD), and should be of significance in the microelectronic industry.

Acknowledgement

This work is supported by the "Research for the Future" Program from the Japan Society for the Promotion of Science, the Natural Science Foundation of China, the Educational Ministry of China, and the Fok Ying Tung Education Foundation.

[1] *VLSI Technology* (Ed.: S. M. Sze), McGraw – Hill, Singapore, **1984**.
[2] J. C. Anderson, *J. Vac. Sci. Technol.* **1986**, *A4*, 610 – 616.
[3] K. D. Wise, *J. Vac. Sci. Technol.* **1986**, *A4*, 617 – 622.
[4] F. Bozso, Ph. Avouris, *Phys. Rev. Lett.* **1986**, *57*, 1185 – 1188.
[5] Ph. Avouris, F. Bozso, R. J. Hamers, *J. Vac. Sci. Technol.* **1987**, *B5*, 1387 – 1392.
[6] R. J. Hamers, Ph. Avouris, F. Bozso, *J. Vac. Sci. Technol.* **1988**, *A6*, 508 – 511.
[7] F. Bozso, Ph. Avouris, *Phys. Rev.* **1988**, *B38*, 3937 – 3942.
[8] J. L. Bischoff, F. Lutz, D. Bolmont, L. Kubler. *Surf. Sci.* **1991**, *251/252*, 170 – 174.
[9] L. Kubler, J. L. Bischoff, D. Bolmont, *Phys. Rev.* **1988**, *B38*, 13113 – 13123.
[10] M. Fujisawa, Y. Taguchi, Y. Kuwahara, M. Onchi, M. Nishijima, *Phys. Rev.* **1989**, *B39*, 12918 – 12920.
[11] C. U. S. Larsson, A. S. Flodstrom, *Surf. Sci.* **1991**, *241*, 353 – 356.
[12] P. J. Chen, M. L. Colaianni, J. T. Yates, Jr. *Surf. Sci.* **1992**, *214*, L605 – L610.
[13] M. J. Dresser, P. A. Taylor, R. M. Wallace, W. J. Choyke, J. T. Yates, Jr. *Surf. Sci.* **1989**, *218*, 75 – 107.
[14] X.-L. Zhou, C. R. Flores, J. M. White, *Surf. Sci.* **1992**, *268*, L267 – L273.
[15] N. Franco, J. Avila, M. E. Davila, M. C. Asensio, D. P. Woodruff, O. Schaff, V. Fernandez, K.-M. Schindler, V. Fritzsche, A. M. Brandshaw, *Phys. Rev. Lett.* **1997**, *79*, 673 – 676.
[16] A. Glachant, D. Saidi, *J. Vac. Sci. Technol.* **1985**, *B3*, 985 – 991.
[17] J. L. Bischoff, L. Kubler, D. Bolmont, *Surf. Sci.* **1989**, *209*, 115 – 130.
[18] J. Stober, B. Eisenhut, G. Rangelov, Th. Fauster, *Surf. Sci.* **1994**, *321*, 111 – 126.
[19] R. H. Zhou, P. L. Cao, S. B. Fu, *Surf. Sci.* **1991**, *249*, 129 – 137.
[20] N. W. Moriarty, P. V. Smith, *Surf. Sci*. **1992**, *265*, 168 – 174.
[21] E. Fattal, M. R. Radeke, G. Reynolds, E. A. Carter, *J. Phys. Chem*. **1997**, *B101*, 8658 – 8661.
[22] R. Miotto, G. P. Srivastava, A. C. Ferraz, *Phys. Rev*. **1998**, *B58*, 7944 – 7949.
[23] S. H. Lee, M. H. Kang, *Phys. Rev*. **1998**, *B58*, 4903 – 4908.
[24] Y. Widjaja, M. M. Mysinger, C. B. Musgrave, *J. Phys. Chem*. **2000**, *B104*, 2527 – 2533.
[25] Z. H. Loh, H. C. Kang, *J. Chem. Phys.* **2000**, *112*, 2444 – 2451.
[26] Y. Widjaja, C. B. Musgrave, *Surf. Sci*. **2000**, *469*, 9 – 20.
[27] X. Xu, S.-Y. Kang, T. Yamabe, *Bull. Chem. Soc. Jpn*. **2001**, *14*, 817 – 825.
[28] A. D. Becke, *J. Chem. Phys.* **1993**, *98*, 5648 – 5652.
[29] C. Lee, W. Yang, R. G. Parr, *Phys. Rev*. **1998**, *B37*, 785 – 789.
[30] L. A. Curtiss, K. Raghavachari, P. C. Redfern, J. A. Pople, *J. Chem. Phys.* **1997**, *106*, 1063 – 1079.
[31] P. Nachtigall, K. D. Jordan, C. Sosa, *J. Phys. Chem*. **1993**, *97*, 11666 – 11672.
[32] M. M. Francl, W. J. Pietro, W. J. Hehre, J. S. Binkley M. S. Gorden, D. J. Defrees, J. A. Pople, *J. Chem. Phys*. **1982**, *77*, 3654 – 3665.
[33] P. C. Hariharan, J. A. Pople, *Theor. Chim. Acta*, **1973**, *28*, 213 – 222.
[34] T. H. Dunning, Jr. *J. Chem. Phys.* **1989**, *90*, 1007 – 1023.
[35] R. A. Kendall, T. H. Dunning, Jr. R. J. Harrison, *J. Chem. Phys*. **1992**, *96*, 6796 – 6806.
[36] D. E. Woon, T.-H. Dunning, Jr. *J. Chem. Phys.* **1993**, *98*, 1358 – 1371.
[37] *Gaussian 98* (Revision A.5), M. J. Frisch, G. W. Trucks, H. B. Schlegel, G. E. Scuseria, M. A. Robb, J. R. Cheeseman, V. G. Zakrzewski, J. A. Montgomery, Jr. R. E. Stratmann, J. C. Burant, S. Dapprich, J. M. Millam, A. D. Daniels, K. N. Kudin, M. C. Strain, O. Farkas, J. Tomasi, V. Barone, M. Cossi, R. Cammi, B. Mennucci, C. Pomelli, C. Adamo, S. Clifford, J. Ochterski, G. A. Petersson, P. Y. Ayala, Q. Cui, K. Morokuma, D. K. Malick, A. D. Rabuck, K. Raghavachari, J. B. Foresman, J. Cioslowski, J. V. Ortiz, B. B. Stefanov, G. Liu, A. Liashenko, P. Piskorz, I. Komaromi, R. Gomperts, R. L. Martin, D. J. Fox, T. Keith, M. A. Al-Laham, C. Y. Peng, A. Nanayakkara, C. Gonzalez, M. Challacombe, P. M. W. Gill, B. Johnson, W. Chen, M. W. Wong, J. L. Andres, C. Gonzalez, M. Head-Gordon, E. S. Replogle, J. A. Pople, Gaussian, Inc., Pittsburgh PA, **1998**.
[38] T. Takaoka, I. Kusunoki, *Surf. Sci*. **1998**, *412/413*, 30 – 41.
[39] H. Over, J. Wasserfall, W. Ranke, C. Ambiatello, R. Savitzki, D. Wolf, W. Moritz, *Phys. Rev*. **1997**, *B55*, 4731 – 4736.
[40] *CRC Handbook of Chemistry and Physics*, 76th ed, (Ed: D. R. Lide), CRC Press, New York, **1995**.
[41] C. J. Wu, I. V. Ionova, E. A. Carter, *Surf. Sci*. **1993**, *295*, 64 – 78.
[42] P. Nachtigall, K. D. Jordan, *J. Chem. Phys.* **1994**, *101*, 2648 – 2649.
[43] U. Höfer, L. Li, T. F. Heinz, *Phys. Rev.* **1992**, *B45*, 9485 – 9488.
[44] M. R. Radeke, E. A. Carter, *Phys. Rev.* **1996**, *B54*, 11803 – 11817.
[45] C. J. Wu, E. A. Carter, *Phys. Rev.* **1992**, *B46*, 4651 – 4658.
[46] K. Sinniah, M. G. Sherman, L. B. Lewis, W. H. Weinberg, J. T. Yates, Jr. K. C. Janda, *J. Chem. Phys.* **1990**, *92*, 5700 – 5711.
[47] M. L. Wise, B. G. Koehler, P. Gupta, P. A. Coon, S. M. George, *Surf. Sci.* **1991**, *258*, 166 – 176.
[48] M. C. Flowers, N. B. H. Jonathna, Y. Liu, A. Morris, *J. Chem. Phys.* **1993**, *99*, 7038 – 7048.
[49] F. M. Zimmermann, X. Pan, *Phys. Rev. Lett.* **2000**, *85*, 618 – 621.
[50] M. Dürr, Z. Hu, A. Biedermann, U. Höfer, T. F. Heinz, *Phys. Rev. Lett.* **2002**, *88*, 046104.
[51] M. Dürr, U. Höfer, *Phys. Rev. Lett.* **2002**, 88, 076107.
[52] A. A. Bagatur'yants, K. P. Novoselov, A. A. Safonov, J. V. Cole, M. Stoker, A. A. Korkin, *Surf. Sci*. **2001**, *486*, 213 – 225.
[53] C. Bater, M. Sanders, J. H. Craig, Jr. *Surf. Interface Anal*. **2000**, *29*, 208 – 214.

Received: January 14, 2002
Revised: August 1, 2002 [F3793]

